

Mitigating RGB-D camera errors for robust ultrasonic inspections using a force-torque sensor

Morteza Tabatabaeipour, William Jackson, Adam Gilmour, Dayi Zhang, Alastair Poole, Konstantinos Tzaferis, Gordon Dobie & Anthony Gachagan

To cite this article: Morteza Tabatabaeipour, William Jackson, Adam Gilmour, Dayi Zhang, Alastair Poole, Konstantinos Tzaferis, Gordon Dobie & Anthony Gachagan (06 Aug 2024): Mitigating RGB-D camera errors for robust ultrasonic inspections using a force-torque sensor, Nondestructive Testing and Evaluation, DOI: [10.1080/10589759.2024.2386618](https://doi.org/10.1080/10589759.2024.2386618)

To link to this article: <https://doi.org/10.1080/10589759.2024.2386618>



© 2024 The Author(s). Published by Informa UK Limited, trading as Taylor & Francis Group.



Published online: 06 Aug 2024.



Submit your article to this journal [↗](#)




View related articles [↗](#)



View Crossmark data [↗](#)

Mitigating RGB-D camera errors for robust ultrasonic inspections using a force-torque sensor

Morteza Tabatabaeipour^a, William Jackson^b, Adam Gilmour^b, Dayi Zhang ^b, Alastair Poole^b, Konstantinos Tzaferis^b, Gordon Dobie^b and Anthony Gachagan^b

^aSchool of Engineering, Ulster University, Belfast, UK; ^bCentre for Ultrasonic Engineering (CUE), University of Strathclyde, Glasgow, UK

ABSTRACT

Robot-based phased array ultrasonic testing is widely used for precise defect detection, particularly in complex geometries and various materials. Compact robots with miniature arms can inspect constrained areas, but payload limitations restrict sensor choice. RGB-D cameras, due to their small size and light weight, capture RGB colour and depth data, creating colourised 3D point clouds for scene representation. These point clouds help estimate surface normals to align the ultrasound transducer on complex surfaces. However, sole reliance on RGB-D cameras can lead to inaccuracies, affecting ultrasonic beam direction and test results. This paper investigates the impact of transducer pose and RGB-D camera limitations on ultrasonic inspections and proposes a novel method using force-torque sensors to mitigate errors from inaccurately estimated normals from the camera. The force-torque sensor, integrated into the robot end effector, provides tactile feedback to the controller, enabling joint angle adjustments to correct errors in the estimated normal. Experimental results show the successful application of ultrasound transducers using this method, even with significant misalignment. Adjustments took approximately 4 seconds to correct deviations from 12.55°, with an additional 4 seconds to ensure the probe was parallel to the surface, enhancing ultrasonic inspection accuracy in complex, constrained environments.

ARTICLE HISTORY

Received 11 December 2023
Accepted 23 July 2024

KEYWORDS

Robotics in hazardous fields; RGB-D perception; force and tactile sensing; force control; phased array ultrasonic inspection; misalignment correction

1. Introduction

The utilisation of welded joints is widespread across critical and demanding sectors, including nuclear, oil and gas, maritime, petrochemical, construction, and transportation industries. These joints frequently serve as sources of structural failures, which can entail significant health and safety hazards. Enhancing industrial maintenance involves reducing costs and the potential for human error [1]. Regular inspections using reliable and efficient ultrasonic techniques [2] are imperative to ensure sustained structural integrity. However, these joints are often situated in hard-to-reach or hazardous environments, such as those within the nuclear sectors [3,4]. Moreover, the

CONTACT Morteza Tabatabaeipour  m.tabatabaeipour@ulster.ac.uk

© 2024 The Author(s). Published by Informa UK Limited, trading as Taylor & Francis Group.

This is an Open Access article distributed under the terms of the Creative Commons Attribution License (<http://creativecommons.org/licenses/by/4.0/>), which permits unrestricted use, distribution, and reproduction in any medium, provided the original work is properly cited. The terms on which this article has been published allow the posting of the Accepted Manuscript in a repository by the author(s) or with their consent.

welded joints themselves may have intricate geometries, requiring highly specialised inspectors and dedicated inspection equipment. Assessing complex geometries often involves semi-automated techniques, which require significant setup and dismantling procedures. This leads to extended labour hours and potential downtime. Traditional phased array ultrasonic testing (PAUT) systems, while effective, often face challenges with probe alignment due to surface irregularities and dynamic operational conditions. Although PAUT probe fixtures in the oil and gas industry are typically spring-loaded to ensure the probe sits flush to the surface, misalignments can still occur due to surface irregularities, wear and tear of fixtures, and dynamic operational conditions. To address these challenges, robotic platforms have been employed to navigate and conduct inspections in demanding environments [2,5–8]. These robotic platforms offer significant advantages, notably by eliminating the need for personnel to physically access the site. This is particularly advantageous in scenarios where site access is costly, hazardous (e.g. hot areas within a nuclear site), requires rope access, or involves confined spaces that demand significant ventilation before inspections can occur.

Ensuring that the ultrasound waves are properly received in robotic ultrasonic systems requires precise alignment of the probe on the component during inspection. This has been studied by Zhang et al. [9]. They examined the constraints of transducer alignment and Unmanned Aerial Vehicle (UAV) stability in the airborne ultrasonic inspection of structural assets. They reported using an onboard laser scanner to provide real-time measurements of UAV alignment and standoff errors relative to the sample's surface normal vector. Additionally, for medical ultrasound applications, Ma et al. [10] developed an end-effector design that enables self-adjustment of the medical ultrasound probe's position. They incorporated four laser distance sensors into the end-effector to estimate the required rotation towards the normal direction. Similarly, three laser sensors based on the same concept have been reported for Non-Destructive Testing (NDT) applications [6].

The use of force-torque sensors has been proven to provide effective tactile feedback to the end effector in robotic ultrasonic inspection systems, enhancing accuracy through real-time adjustments of the transducer. Jiang et al. reported a force-based technique to estimate the probe orientation without requiring visual features to achieve automatic orthogonal positioning of a medical ultrasound probe relative to the tissue surface [11]. Two rotations are performed along orthogonal axes while recording the contact force. Subsequently, the force data is fed into a mechanical model to estimate the normal direction. Recently, a technique for robotised ultrasonic testing has been reported. This technique can plan and execute collision-free scans over surfaces without the need for computer-aided design files or extensive pre-scanning via lasers on composite structures [5]. This approach leverages RGB-D cameras, extending their application in robotic NDT. Furthermore, the method integrates real-time sensor adjustments for the robot's position and movement directions, significantly improving the transition from isolated corrections to comprehensive part coverage, even within the constraints of limited data. This approach addressed the challenges posed by inspecting intricate geometries in demanding environments, demonstrating potential for enhanced safety and efficiency within the industry.

RGB-D cameras, which capture both colour and depth information, can provide geometrical information and point cloud data of the component under inspection. The cameras offer several significant advantages. Firstly, they provide high-resolution colour and depth information, which is crucial for detailed environmental mapping and object recognition [12]. Additionally, these cameras are capable of real-time data processing, making them essential for dynamic and responsive systems [13]. Their cost-effectiveness, compared to other 3D sensing technologies, makes them accessible for a wide range of applications. Moreover, RGB-D cameras are generally easy to integrate with existing systems and software, facilitating their use in various research setups. Accurate surface normal estimation could also be useful for robotic approach and ultrasound coupling.

Despite their potential, the use of RGB-D cameras in robotic inspections is not without its challenges. They are restricted by their limited range and field of view, which can hinder their effectiveness in larger or more complex environments. Furthermore, these cameras can be sensitive to lighting variations, affecting the accuracy and reliability of the data collected. The point cloud can also be noisy, particularly at the edges of objects or in low-contrast scenes, posing challenges for precise measurements. The quality of point cloud data from these cameras can significantly influence the proper orientation of a phased array ultrasound probe during the inspection. Consequently, the accuracy of the surface normal estimation in noisy points becomes critical [14].

Several studies have evaluated the accuracy of the Intel RealSense RGB-D cameras across various applications. These investigations have utilised a combination of planar and spherical artefacts [15], along with more exotic shapes [16,17] to assess the system's accuracy for specific use-cases, such as profiling and medical applications. Studies focusing on Intel RealSense RGB-D cameras have provided insights into their practicality and constraints. Despite their success in various applications, these cameras exhibit limitations in accurately estimating normals on reflective metallic surfaces, a characteristic feature often encountered in NDT applications.

[18] presented a novel technique using texture synthesis methods guided by segmented RGB images to address some of these RGB limitations. The technique has been developed to rectify depth holes and missing data in depth images captured by Intel RealSense D435i RGB-D cameras. Through the application of a texture synthesis method guided by segmented RGB images, accurate filling of absent depth data occurs. This preserves object boundaries and more effectively mitigates errors across depth discontinuities. Quantitative assessments employing metrics like root mean square error (RMSE), peak signal-to-noise ratio (PSNR), and structural similarity index measure (SSIM) further validate its efficacy in surmounting the constraints of RGB-D cameras. Notably, it enhances their applicability in tasks such as 3D reconstruction.

Another study [19] has contributed significant insights into the measurement of depth resolution in Intel RealSense RGB-D cameras. This study introduces a novel approach that involves generating a stair-shaped depth map by gradually advancing the camera towards a flat target. It unveils a minimum detectable depth difference of 0.5 mm for RealSense D455 and 1–2.5 mm for D435. Beyond identifying influential factors on resolution, this research presents a reliable technique for circumventing the challenges associated with direct depth resolution measurement. It also facilitates the characterisation of RGB-D camera performance [19].

Ahn et al. [20] have also undertaken a comprehensive analysis of the performance of the Intel RealSense D435 RGB-D camera in the realm of robotic applications. Their investigation focuses on systematic errors, particularly addressing issues like distance inhomogeneity and depth bias. Moreover, the researchers formulated a model for the random noise in depth values, employing a Gaussian distribution. This modelling revealed that axial noise exhibits a quadratic trend, while lateral noise remains relatively constant due to constraints originating from stereo image overlap. It is important to note that a significant constraint arises from the presence of missing or noisy depth values on one side due to the stereo camera baseline. This factor presents challenges in accurately modelling lateral noise.

Additionally, the work authored by Jonasson et al. [21] performs a comparative evaluation of three fundamental sensing technologies within the realm of robotics: RGB-D camera, LiDAR (light detection and ranging) sensor, and Millimetre-Wave radar. The study specifically focuses on their applicability in nuclear maintenance scenarios. The primary outcomes highlight certain limitations of RGB-D cameras, including a relatively shorter range. However, these cameras exhibit the capability to generate high-density data. As a result, the research positions these three sensors as complementary components that, when combined, contribute to improved overall performance and redundancy within the context of nuclear maintenance applications.

Force-torque sensors are crucial in a variety of industrial applications [22], due to their precise force and torque measurement capabilities. Their high resolution and accuracy are essential for tasks requiring detailed feedback and control, such as delicate assembly, surgical robotics, and interactions with unpredictable environments. By integrating force-torque sensors on a robot's end effector, real-time tactile feedback is provided, allowing the system to dynamically adjust and correct the probe's position. This ensures optimal contact with the inspection surface, enhancing the quality of ultrasonic data collected.

These sensors measure contact force and torque, enabling precise control and correction of the probe's orientation, which is particularly important for inspecting intricate welded joints in constrained and hazardous environments. Although RGB-D cameras effectively generate point clouds for surface normal estimation, they are prone to inaccuracies caused by noise and environmental factors, leading to potential misalignment of the ultrasound transducer. Force-torque sensors help correct errors in estimated normals from RGB-D cameras, improving the alignment of the ultrasonic beam and the overall quality of inspection results. Research has shown that tactile feedback from force-torque sensors can significantly reduce misalignment errors [22], thus enhancing the performance of robotic inspection systems.

2. Aim and objectives

The research goal of this paper is to create a compact-size robot for inspecting assets in constrained areas with limited access, utilising ultrasound phased array transducers. It covers well-lit and dark indoor spaces, as well as outdoor environments.

The robot's small size necessitates the use of a miniature robot arm, which leads to payload restrictions. The robot requires remote navigation and localisation using

an onboard camera. 3D mapping of the surrounding environment and assets proves beneficial for remote inspections. RGB-D cameras are useful in such scenarios as they are small and lightweight, rapidly capturing RGB colour and depth data, generating a colourised 3D point cloud for scene representation. This facilitates estimating normal vectors and aligning the ultrasound transducer parallel to the surface, especially for inspection targets with relatively complex geometries. However, the camera's inherent noise and limitations pose challenges in achieving precise transducer alignments. The ultrasound phased array transducers are especially sensitive to misalignment, leading to errors in beamforming and interference. To address this issue, post-processing algorithms, such as fittings [7,23,24], can be applied to the camera data to minimise errors and improve the accuracy of pose estimations. However, these post-processing algorithms often require significant computational resources and may still introduce some level of errors, leading to misalignments.

This article investigates the limitations of using RGB-D cameras and explores a method to address these limitations. The approach involves utilising the force-torque sensor integrated into the robot arm's end-effector for closed-loop tactile feedback control. This approach effectively mitigates the negative impact caused by the camera's limitations. The integration of tactile feedback in conjunction with RGB-D cameras opens new possibilities for more accurate and reliable inspections. It is worth noting that the paper does not propose replacing the camera with the force-torque sensor; rather, it aims to mitigate the errors generated by the camera using the force-torque sensor, particularly where the limitations of RGB-D cameras are significant.

The rationale for this robot is rooted in enhancing safety, efficiency, and accuracy of inspections in industries where welded joints are critical. The robotic arm with the RGBD camera ensures complete and consistent coverage around the weld. The system senses the area around the weld, creates targeted poses for precise manipulation, and applies uniform pressure. By employing a compact robotic arm with advanced sensor integration, the system reduces the need for human intervention in hazardous environments, minimises downtime by enabling quicker setup and execution of inspections, and ensures higher accuracy in defect detection. These advantages are particularly significant in industries like oil and gas, nuclear, and maritime, where maintaining structural integrity is paramount.

The remainder of the paper is structured as follows. [Section 3](#) provides an overview of the compact inspection robot, including its hardware and software components. [Section 4](#) analyses the impact of probe misalignment errors on ultrasound phased array measurements. [Section 5](#) focuses on the limitations of the RGB-D camera under various environmental brightness conditions on industrial assets. [Section 6](#) presents the proposed closed-loop tactile feedback method, which utilises force-torque sensors to mitigate sensor misalignments caused by camera noise and limitations. [Section 7](#) demonstrates the system on an industrial pipe. The system successfully mitigated a 12.55° misalignment in approximately 4 seconds using the proposed method. The paper concludes in [Section 8](#), summarising the key findings and discussing future research work.

The main contributions of this paper are as follows:

- (1) Developed a compact-sized ultrasonic-inspection robot for ultrasound phase array inspections.
- (2) Evaluated the ultrasound phased array transducer alignment requirements.
- (3) Explore the RGB-D camera limitations in various environment brightness conditions.
- (4) Proposed is a closed-loop tactile feedback method utilising force-torque sensors to mitigate sensor misalignments caused by the camera noises and limitations.
- (5) The system is demonstrated on an industrial pipe, successfully mitigating a 12.55° misalignment around 4 seconds using the proposed method.

3. System overview

The inspection system utilised in this paper, as shown in [Figure 1](#), consists of: a Navic Jireh crawler [25], a Meca500 6-degree-of-freedom robot arm [26] with an integrated ATI force-torque sensor [27] on the end effector, a 64-element, 10 MHz ultrasound phased array probe [28], and an Intel RealSense D435i RGB-D camera [13].

The Navic Jireh crawler features a two-axis articulation mechanism, providing independent pitch and roll angles for improved manoeuvrability and traction on surfaces during inspections of pipes and vessels. A Meca500 miniature 6-degree-of-freedom robot arm is installed on the crawler, enabling precise positioning of the sensor payload [7,29]. This combination offers a versatile solution for surface manoeuvring and contact inspections, expanding the robot's applicability and adaptability in diverse conditions. The ATI

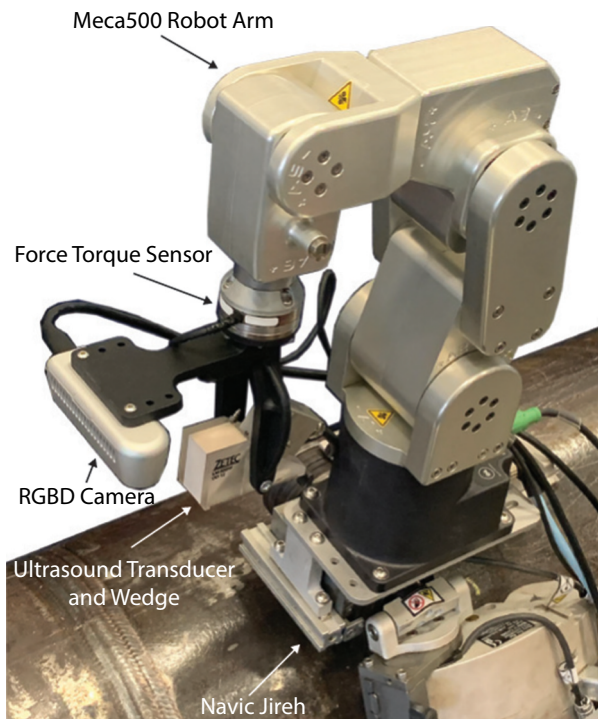


Figure 1. The remote inspection robot for the assessment of complex geometry.

force-torque sensor is integrated on the robot end-effector to precisely measure the contact force and torque applied to the ultrasound transducer. It ensures proper contact force applied to the transducer and maintains optimal coupling. The crawler and robotic arm of the system are controlled based on the software running the Robot Operating System (ROS) [30]. The custom software, including the robot end effector controls, was written as a collection of nodes both in C++ and Python and integrated into the operating system. The software subscribes to data published by the sensors and publishes commands to the other peripherals.

The middleware layer of the inspection system incorporates several key components, as shown in Figure 2. These include visual identification of welded joints, point cloud generation, and the selection of the initial ultrasonic scan point based on the 3D point cloud captured by the RGB-D camera. Point cloud processing is performed to estimate the normal vector at the selected starting point, determined by the robot operator. This information is subsequently utilised to calculate the roll, pitch, and yaw angles for the Meca500 robot at the specified starting point. The robotic arm is moved to the vicinity of the desired point, and it then approaches the component surface using the force-torque sensor.

The 64-element, 10 MHz ultrasound phased array probe is connected to the robot arm through a Zetec DYNARAY phased array controller. The setup includes a 55° shear wave wedge with a surface face having a radius of 162.5 mm matching that of the pipe (as

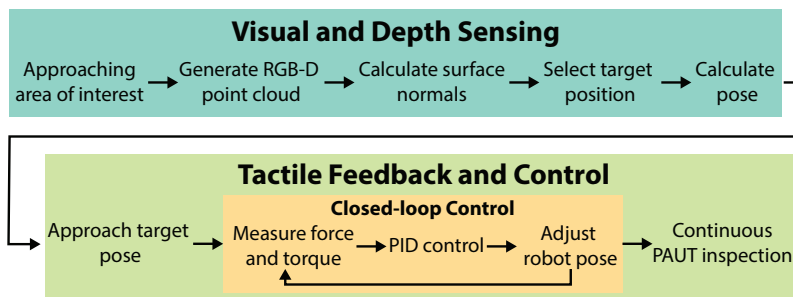


Figure 2. Flowchart of the robotic inspection process with closed-loop feedback control.

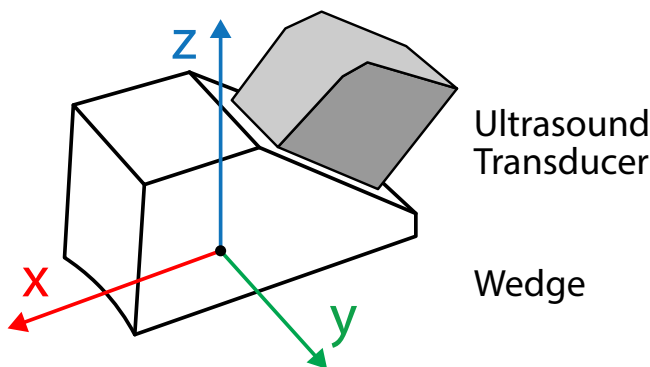


Figure 3. Ultrasound inspection payload coordinate system.

Figure 3), which enhances beam steering, impedance matching, focus control, and artefact reduction, leading to improved ultrasound image quality. The inspection results are recorded and visualised using the UltraVision Software, developed by Zetec [31].

The Intel RealSense D435i RGB-D camera is mounted on the end-effector. The camera utilises stereo depth sensors with infrared light to enhance data accuracy. By comparing images from two sensors with a known distance between them, depth information is extracted as a point cloud. The camera's colour information helps the operator navigate and locate the robot, while the depth data enables precise 3D spatial perception of the inspected component and assists in estimating normal vectors for ultrasound transducer deployments.

To estimate the normal vectors of points in a 3D point cloud, a process involving several steps is employed. Initially, the points within a 2.5 mm radius around each query point, denoted as p_i , are identified as the neighbourhood points. Subsequently, a covariance matrix, denoted as \mathbf{C} , is calculated based on these neighbouring points. The next step involves computing the eigenvalues and eigenvectors of the covariance matrix using the Equation (1) [32].

$$\mathbf{C} = \frac{1}{k} \sum_{i=1}^k (p_i - \bar{p}) \cdot (p_i - \bar{p})^T \quad (1)$$

$$\mathbf{C} \cdot \vec{v}_j = \lambda_j \cdot \vec{v}_j, j \in 0, 1, 2$$

where k represents the number of neighbouring points considered in the local neighbourhood of point p_i . The centroid of these neighbours is denoted as \bar{p} , the eigenvalues of the covariance matrix are represented as λ_j , and the corresponding eigenvectors are denoted as \vec{v}_j .

The eigenvector corresponding to the smallest eigenvalue is considered the surface normal at the desired point. These eigenvalues and eigenvectors carry essential information about the local surface curvature and orientation at each query point, allowing for precise estimation of the normal vectors for the entire 3D point cloud. Next, the normal vectors are used to calculate the roll, pitch, and yaw angles using the Quaternion Representation [33]. These angles are used to create a pose for the Meca500 robot to position the ultrasound transducer.

4. Alignment constraints on ultrasound phased array

Angular misalignment errors in the transducer can cause signal attenuation when its face is not parallel to the surface of the inspection target, as evidenced by practical experience [34,35]. Consequently, this experiment aims to determine the alignment constraints of the transducer and evaluate their impact on the inspection results. Through this study, a quantitative analysis of transducer alignment requirements was conducted, with the aim of comprehensively understanding the implications for achieving accurate and reliable inspection outcomes.

While performing this experiment, the ultrasound transducer was executed, and its outputs were digitised using the Zetec DYNARAY system, as discussed in Section 3. To manipulate the transducer's position, the robot arm was manually controlled, allowing for adjustments within a range of 0° to 3° about the X-axis. Benefiting from the

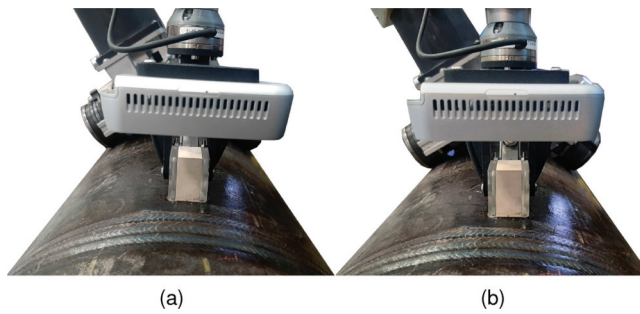


Figure 4. Experiment setup for the quantification of alignment constraints. (a) The probe is parallel to the asset. (b) The probe had 3° alignment deviation to the surface.

mechanical design of the transducer probe mount, as shown in [Figure 1](#), the transducer has one degree of freedom that allows it to rotate about the Y-axis around the mounting hole. This feature offers flexibility, as when the probe contacts the asset, it will self-align against the surface about the Y-axis. Therefore, alignment analysis about the Y-axis is neglected.

During the experiment, the transducer maintained contact with the asset using a layer of couplant gel, as shown in [Figure 4](#). This setup ensured consistent and reliable coupling between the transducer and inspected surface, thereby eliminating signal loss that may arise from poor coupling.

The sector scan results captured by the transducer under different alignment errors are shown in [Figure 5](#). When the transducer was parallel to the surface, the welded joints exhibited the highest reflections, as shown in the [Figure 5\(a\)](#). Specifically, the amplitude from the root of the welded joint measured approximately 9000 in this scenario.

The observed increase in signal attenuation as the transducer deviates from the normal alignment emphasises the critical relationship between the transducer alignment angle and the accuracy of the inspection process. Significant signal attenuation was observed when the transducer's alignment angle exceeded 2°. Therefore, it can be deduced that a maximum alignment offset of 2° can be reasonably tolerated while still obtaining satisfactory reflection signals. These findings highlight the importance of maintaining precise alignment to ensure reliable and accurate inspection results.

5. RGB-D camera limitations on environment brightness

As observed in various literature [[36–38](#)], brightness is crucial for RGB-D cameras as it directly impacts the accuracy and quality of depth measurements. In low-light conditions, the camera's ability to capture accurate colours is compromised. The images appear grainy, less sharp, and have dull or distorted colours. Excessive environmental brightness can also negatively impact camera performance. Overexposure can lead to the loss of detail and saturation in RGB images captured by the camera sensor. Furthermore, strong ambient light can interfere with the infrared illumination used for cameras' depth sensing, causing depth errors or occlusions in the point cloud.

This experiment aims to determine the accuracy of the RGB-D camera under various environmental brightness conditions. The experiment was conducted in a laboratory

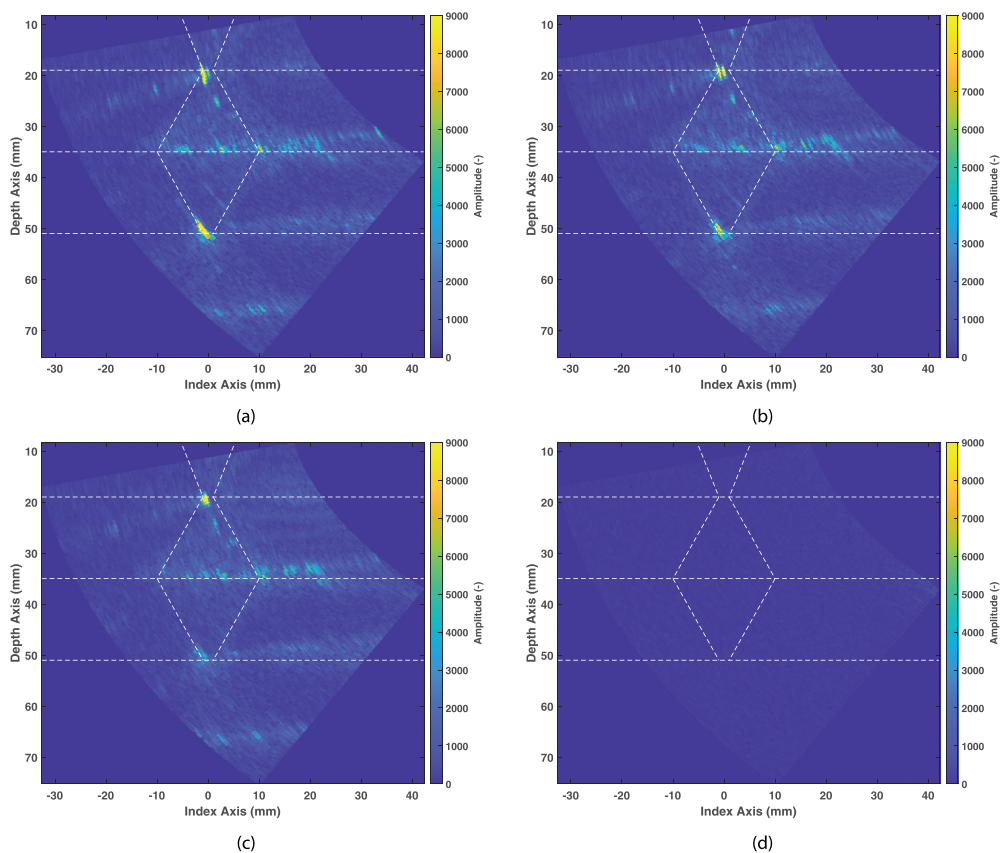


Figure 5. The sector scan with the alignment error of, (a) 0° , (b) 1° , (c) 2° , (d) 3° .

setting, enabling precise control of ambient light levels using supplementary lighting. Throughout the experiment, the RGB-D camera was positioned approximately 270 mm away from the top surface of the 325 mm outer diameter mild steel pipe, as shown in [Figure 6](#).

The camera resolution for this experiment was set at 848×480 pixels, corresponding to the minimum operating distance of 195 mm [39]. The camera exposure settings were configured to the factory defaults. The depth format was set to Z16, and the laser emitter was enabled with a power of 150 mW. Within the laboratory and without additional illumination, the light intensity was measured using a calibrated lux meter, yielding a value of 170 lx.

The first set of data was captured under normal room lighting conditions, simulating inspections conducted in well-lit indoor environments. The second set of data was captured with additional lighting applied to the side of the pipe (500 lx), simulating inspections conducted in outdoor environments with strong directional lighting. The third set of data was captured in a dark laboratory environment, simulating inspections conducted in indoor environments without any lighting, resulting in a brightness level of approximately 7 lx.



Figure 6. The 325 mm outer diameter mild steel pipe used for RGB-D brightness limitations experiment.

The results of the three test conditions are shown in [Figure 7](#). As shown in [Figure 7\(a\)](#) and [7\(b\)](#), when the camera captured an overexposed area, the intense brightness interferes with the infrared light pattern, resulting in a weakened or distorted signal reflected to the camera sensor, leading to occlusions in the corresponding point cloud. In contrast, when the camera was positioned in the dark room, the point cloud was the most complete, with minimal occlusions. Nevertheless, as depicted in [Figure 7\(c\)](#), the colour information was entirely distorted. Even after image post-processing with enhanced brightness ([Figure 7\(d\)](#)), the colour remained severely altered.

Compared with the point cloud gathered in a dark room as a reference, the occluded area under normal room conditions constitutes approximately 5.7% of the total surface area. However, when additional lighting is introduced, the occluded area expands to approximately 18.7% of the total surface area.

6. Error mitigation using force-torque sensor

Improper alignment of the ultrasound probe can lead to reduced signal penetration, errors in interpretation, and potential misdiagnosis, making it crucial to maintain proper alignment for reliable results and to prevent damage. The misalignment causes uneven force and torque at the end of the robot arm, leading to higher forces on the misaligned transducer compared to a properly aligned one. To address this, the force-torque sensor on the robot's end effector is used to provide tactile feedback during interactions between the ultrasound transducer and inspection surface, allowing for adjustments to correct the alignment.

A Proportional-Integral-Derivative (PID) controller, is a feedback control mechanism widely used in robotics and engineering applications to regulate a system's output. It continuously monitors the error between a desired contact force (setpoint) and the actual measured contact force from the force-torque sensor and adjusts the system's input accordingly.

As [Figure 8](#), the transducer is placed on top of the inspection target using the orientation derived from the raw point cloud, which may contain some misalignment.

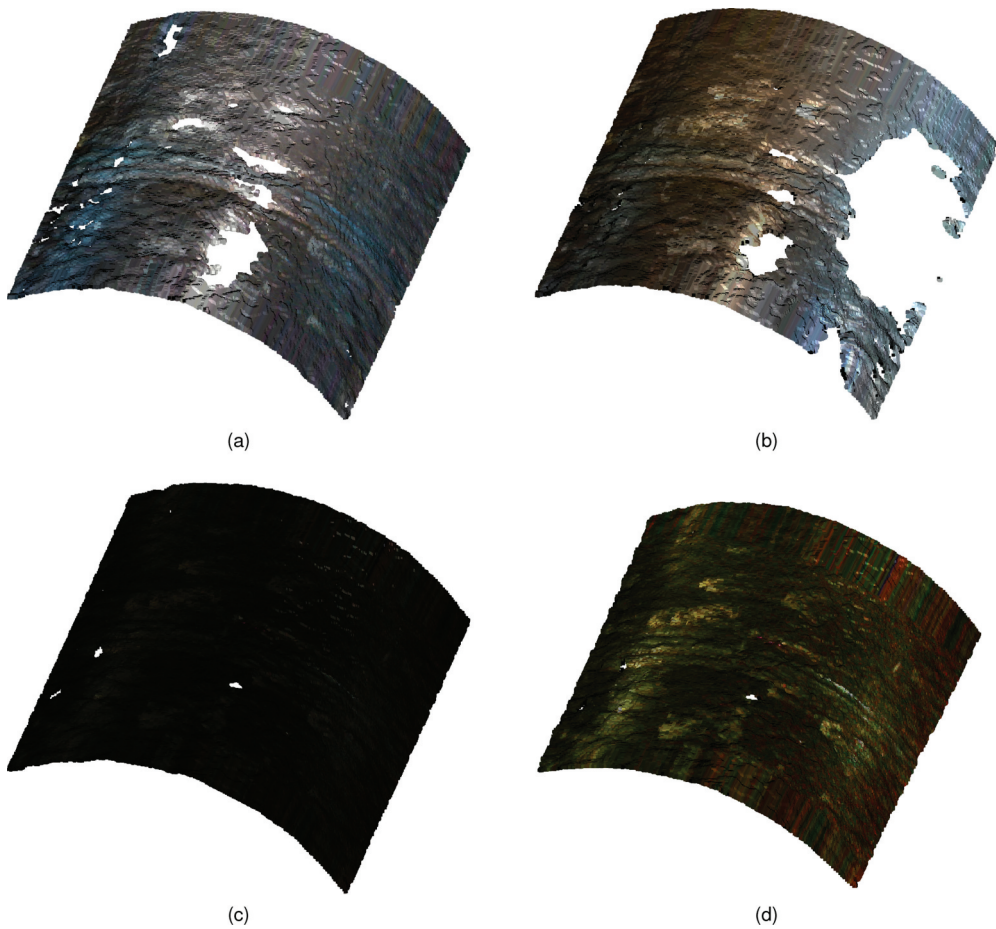


Figure 7. Effects of environmental brightness on the captured point cloud from a mild steel pipe using a RealSense camera. (a) Normal room lighting conditions. (b) Additional lighting from the right side of the pipe. (c) Complete darkness with all lights turned off. (d) Result captured in the dark room with artificially enhanced brightness.

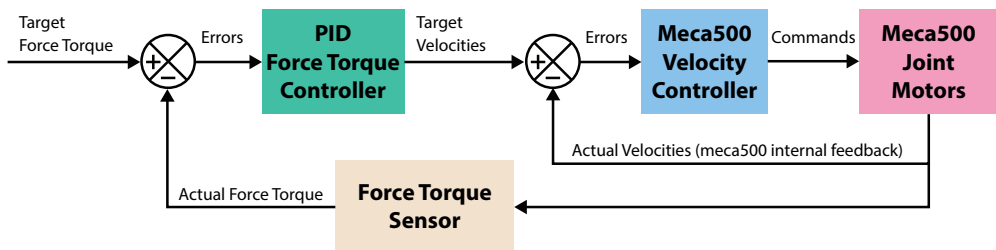


Figure 8. A block diagram of a control system is presented, showcasing the utilisation of closed-loop feedback from the sensor to maintain the contact force and torque applied to the transducer.

The misalignment creates an imbalance of force and torque at the end of the robot arm, resulting in higher forces exerted on the misaligned transducer compared to a properly aligned one. The controller uses the actual force ($F_{measured}$), measured by the force-torque sensor, subtracted by the target force (F_{target}) to calculate the error ($e(t)$) as Equation (2). It then applies proportional control to generate a control signal. The proportional gain determines the magnitude of the corrective action. To eliminate steady-state errors, the integral control component is incorporated. The integral term accumulates the error over time and adjusts the control signal accordingly. This helps the controller address deviations from the desired force. As Equation (3), the combined control signal or target velocities ($u(t)$) is subsequently applied to the robot's internal velocity controller, allowing it to adjust the joint motors, ensure the forces are balanced, and align the probe properly against the surface.

$$e(t) = F_{target} - F_{measured} \quad (2)$$

$$u(t) = K_p e(t) + K_i \int_0^t e(t) dt + K_d \frac{de}{dt} \quad (3)$$

where K_p , K_i and K_d represent the proportional, integral, and derivative gains.

Similarly, a PID controller is also utilised to ensure that the torque applied to the ultrasound transducer closely matches the desired value. The controller calculates the error by comparing the desired torque (setpoint) with the measured torque obtained from the torque sensor.

To optimise the ultrasound probe configuration, a force setting of 12N was chosen to maintain stable contact without signal distortion, ensuring effective ultrasound transmission and preventing excessive friction. A torque setting of 0 Nm was selected to prevent angular movement, keeping the probe stationary and its orientation consistent. These parameters ensure efficient operation, with managed linear and angular velocities preventing deviations. The empirical approach to determining these settings tailors the system to specific operational conditions, maximising the effectiveness and reliability of ultrasound assessments.

7. Practical ultrasound phased array inspection

7.1. Experimental setup

In this experiment, the robot system demonstrated its versatility in conducting a mock ultrasonic inspection. The chosen test subject, a 325 mm diameter mild steel pipe, presented a realistic scenario to assess the capabilities of the robot system. The environment brightness was around 170 lx. The camera settings were the same as described in Section 5. The ultrasonic system was calibrated using a mild steel block (S275) with dimensions of 300 mm × 300 mm × 40 mm, chosen to match the inspected components' material properties. The calibration block included machined defects, providing reference points for signal calibration. The system was calibrated using this block to establish baseline measurements, adjusting settings such as gain and focus to normalise the signal response to a predefined target. The calibration was verified by comparing measured signals with expected values and ensuring

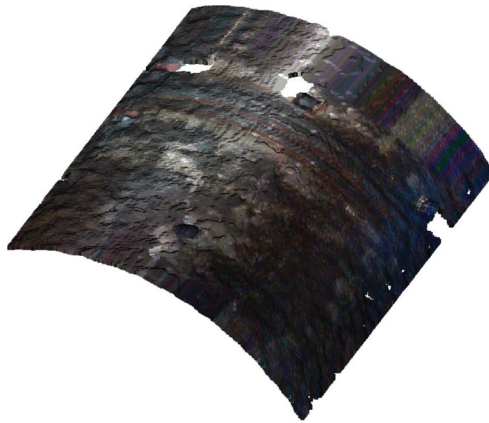


Figure 9. Point cloud generated by the RGB-D camera on the mild steel pipe.

repeatability through multiple calibration runs, thereby ensuring the accuracy and reliability of the inspection results.

First, the RGB-D camera conducted a 3D scan of the pipe, creating a 3D point cloud, as shown in [Figure 9](#). Next, the point cloud data were processed to calculate the approximate required pose of the ultrasound transducer. Using this approximation, the Meca500 robot arm deployed the transducer. During the process, the force-torque sensor, integrated into the arm's end-effector measured the force and torque in real-time, provides tactile feedback to the PID controller. This feedback was used to adjust the orientation and ensure the transducer was properly aligned with the pipe surface. In addition, the ultrasound phased array results were recorded via the Zetec DYNARAY phased array controller.

The values of 10 and 5 were tuned for K_p and K_i , 0 for K_d in both force and torque controllers. Using these specific values, the force and torques controllers effectively combine the proportional and integral terms to balance the transducer and align it properly against the surface.

7.2. Normal error quantification

As demonstrated in the preceding sections, the camera's point cloud exhibits numerous errors that can subsequently impact the accuracy of normal estimation. This section will evaluate the accuracy of normal estimation using the camera's point cloud.

A ground truth point cloud was measured using a FARO Quantum ScanArm with Laser Line scanner [40], represented in green in [Figure 10\(a\)](#). The CloudCompare software [41] was used to calculate discrepancies between the point-clouds generated by the camera and those scanned by the laser arm, as illustrated in [Figure 10\(b\)](#). The analysis revealed a maximum distance deviation of approximately 3.4 mm, predominantly occurring along the top and bottom edges of the region of interest. The deviation exhibited a direct correlation with the absolute distance between the point on the pipe surface and the camera position. The point that demonstrated the highest deviation was situated approximately 10 away from the camera.

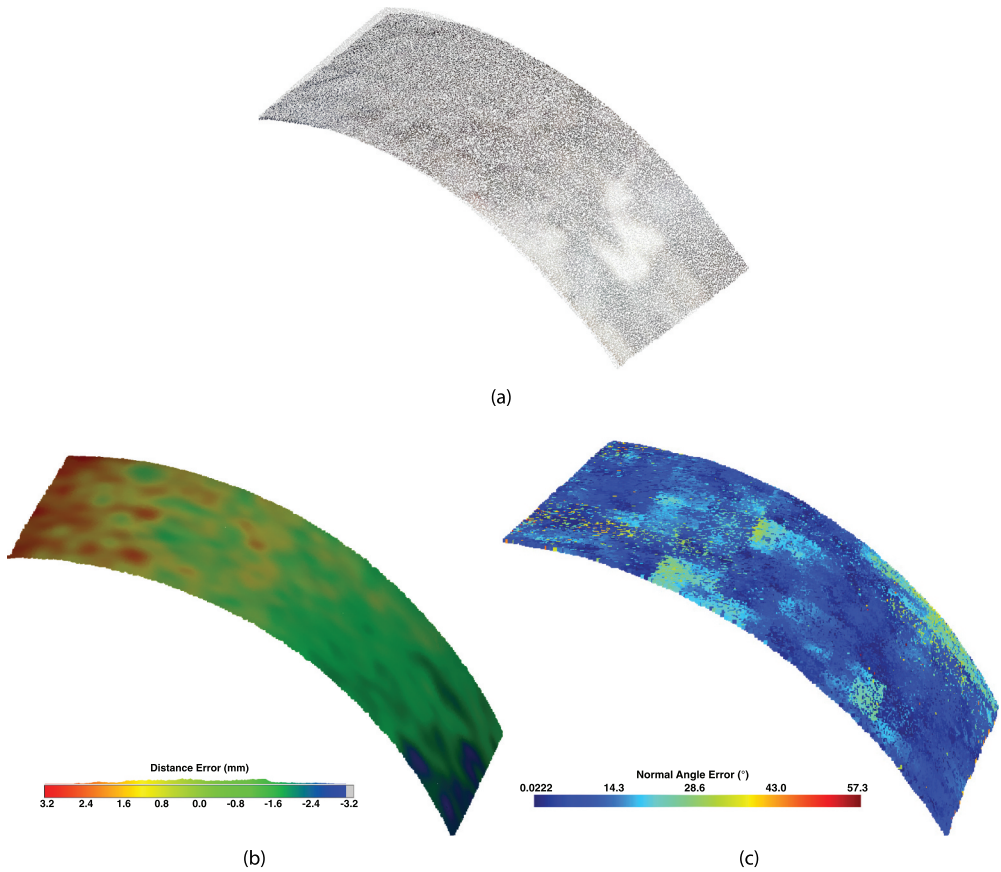


Figure 10. Point cloud comparison: (a) the point cloud generated by the FARO laser scanner and overlaid on top of the RGB-D colour map. (b) The distance error is depicted with the colour bar unit in mm. (c) The angle error is represented with the colour bar unit in degrees.

Figure 10(c) illustrates the angular deviation in degrees for all points in the point cloud generated by the camera. The angular error between the normal vector of point cloud, represented as, n , and the normal vector of the laser, denoted as \hat{n} , was calculated using Equation (4).

$$\text{error} = \arccos\left(\frac{\hat{n} \cdot n}{|\hat{n}| \cdot |n|}\right) \quad (4)$$

The angle errors in degrees are projected onto the camera point cloud. The root mean square angle error between the camera and laser point clouds was 12.55°, as evident in the histogram presented in Figure 11. Certain regions within the point cloud display noticeable abnormal deviations, which can be ascribed to variations in the luminosity of the image captured by the camera. However, it is essential to acknowledge that there are substantial areas in the point cloud where low normal deviation is also observed.

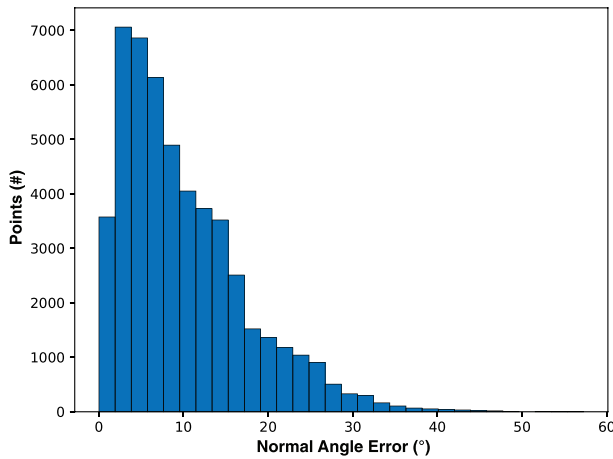


Figure 11. The histogram of the angle error is presented for detailed examination.

7.3. Results and discussions

In this experiment, the focus was on a pipe containing a V-shaped butt weld. To challenge the system and assess its sensitivity, an internal defect in the form of a tungsten insert was intentionally introduced during the welded process. The objective was to determine the system's ability to detect and characterise such flaws, as they can pose critical implications in various industries.

Figures 12–15 demonstrate the progress of this inspection. As shown in Figure 14, there was an initial 12.55° error in deploying the transducer to the pipe surface, likely due to the noise and limitations of the RGB-D camera. The forces and torques at this stage were measured to be above 20N and 0.2 Nm, respectively (as presented in Figure 13). Furthermore, it is hard to identify the welded joint from the ultrasound sector scan (as Figure 15(a)).

The controller successfully adjusted the alignment angles using tactile feedback from the force-torque sensor, as demonstrated in Figure 14. By precisely adjusting the force and torque applied to the transducer, the controller took approximately 4 seconds to reduce the alignment error from 12.55° to the angle within the operational range where

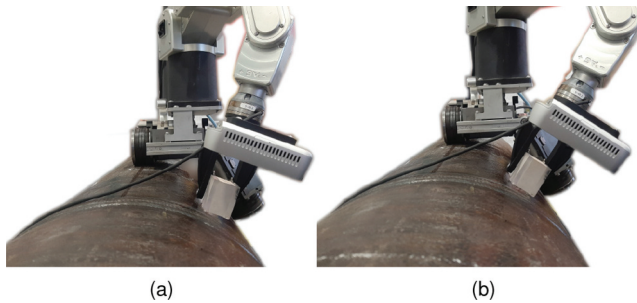


Figure 12. The probe mitigation adjustment process. The probe was moved from 12.55° alignment error (a) to 0° (b), corrected by the controller.

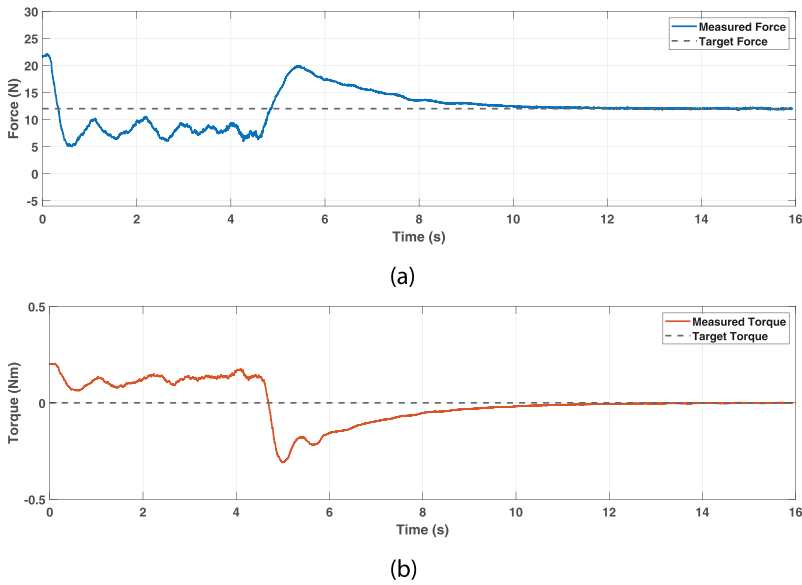


Figure 13. The force (a) and torque (b) applied on the transducer, measured by the force-torque sensor during the alignment mitigation process.

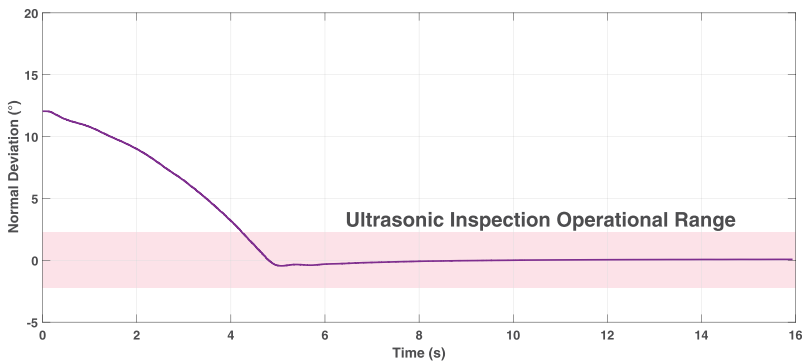


Figure 14. Alignment error versus time during the alignment mitigation process.

the transducer can obtain meaningful results (2°). An additional 4 seconds were used to ensure the probe was perfectly parallel to the surface.

When the ultrasound transducer was properly aligned with the pipe surface, the system successfully detected significant features, including the weld root, and accurately captured the embedded defect, as indicated in Figure 15. The precise alignment, achieved through the feedback-controlled adjustments, allowed the system to obtain high-quality ultrasound data, leading to the successful identification and visualisation of critical details in the inspected pipe. The results highlighted the system successfully detected significant features, including the weld root, and accurately captured the embedded defect.

Overall, the proposed method using force-torque sensors to correct the misalignment of the ultrasound transducer addresses several critical limitations of relying solely on

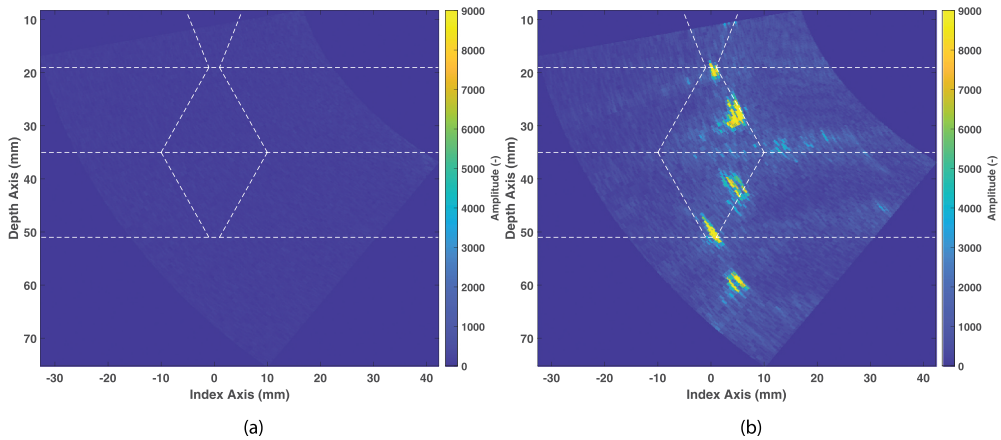


Figure 15. Ultrasound phased array sector scan results, a) 12.55° alignment error, b) after correction (0° alignment error).

RGB-D cameras. RGB-D cameras, while useful for initial point cloud generation, often suffer from inaccuracies due to environmental noise and limitations in estimating surface normals, especially on reflective surfaces. These inaccuracies can lead to significant misalignment of the ultrasound transducer, resulting in poor inspection results. This approach integrates tactile feedback from the force-torque sensor, enabling real-time adjustments that correct these inaccuracies. This not only ensures precise alignment of the transducer but also significantly enhances the quality and reliability of the inspection results. Experimental results demonstrate that this method can correct misalignment from 12.55° to near-perfect alignment within approximately 4 seconds, thereby reducing the error to within the operational range necessary for accurate defect detection. This integration of force-torque sensors mitigates the limitations of RGB-D cameras and improves the overall effectiveness and efficiency of robotic ultrasonic inspections.

8. Conclusion

In conclusion, this paper presented an investigation into the challenges of utilising RGB-D cameras for ultrasound transducer positioning in automated phased array ultrasonic inspections. While RGB-D cameras offer the advantages of compactness and rapid data capture, their limitations can lead to inaccuracies in the generated point clouds. Using these point clouds to estimate the ultrasound transducer orientations will affect the direction of the ultrasound beam and, consequently, impact the accuracy of defect detection especially in complex geometries. Experimental analyses showed that the ultrasound transducer's angle was required to be within 2° of the surface normal vector to receive meaningful sector scan signals for inspecting welded joints. This poses a challenge when relying solely on the camera point cloud to estimate the transducer's angle.

To address this challenge, a novel approach was proposed, which utilised the force-torque sensor on the robot end effector. By providing tactile feedback to the controller, it enabled real-time adjustment of joint angles to correct errors in the

estimated surface normal from the RGB-D camera. The practical experimental results demonstrated the effectiveness of this method, even in cases of significant misalignment. The adjustments take around 4 seconds to correct deviations, resulting in enhanced accuracy of defect detection by reducing the misalignment from 12.55° to the angle at which the transducer can conduct meaningful inspections. The results also prove the importance of tactile feedback in mitigating the limitations of relying on a miniature RGB-D camera for transducer positioning. This advancement allows for precise defect detection in complex and constrained environments, where traditional methods may not be feasible due to limited space and payload constraints.

The proposed method is not only grounded in general control principles but is specifically optimised for autonomous NDT applications. By integrating force-torque sensors with a robotic inspection system, the unique challenges posed by autonomous NDT, such as the need for precise alignment and continuous contact, are addressed. Experimental results demonstrate significant improvements in the accuracy of ultrasonic inspections, reducing alignment errors and enhancing defect detection capabilities. This approach highlights the direct applicability and impact of the method in the field of NDT, offering a robust solution for inspecting complex geometries in constrained and hazardous environments. Notably, the method is not limited to ultrasonic inspections deployed by the robot; it can also be used for other contact-based inspections and applications where the robot needs to position its payload parallel to the target surface.

Future work can include enhancing the effectiveness revolving around controller tuning and potential transitions from PID to non-linear control strategies. Advanced optimisation techniques can be explored to fine-tune PID controller parameters, ensuring optimal performance and further reducing the time cost to correct errors.

Overall, the proposed methodology opens new possibilities for robots in challenging scenarios, where precise sensor payload deployment is crucial for certain applications.

Disclosure statement

No potential conflict of interest was reported by the author(s).

Funding

This work was supported by EPSRC “Delivering Enhanced Through-Life Nuclear Asset Management” [EP/R004889/1] in collaboration with Advanced Nuclear Research Centre (ANRC 12-2).

ORCID

Dayi Zhang  <http://orcid.org/0000-0003-4611-4161>

Data availability statement

The raw data are available from the corresponding author upon reasonable request.

Author contributions

Morteza Tabatabaeipour, William Jackson, Adam Gilmour: writing – original draft preparation, review, and editing; formal analysis, and data collection; Dayi Zhang: writing – original draft preparation, review, and editing; Alastair Poole: formal analysis; Konstantinos Tzaferis: data collection; Gordon Dobie, Anthony Gachagan: supervision and funding acquisition.

References

- [1] GlobalSpec. Defective welds pose another setback for this nuclear power plant. [2024 Jul 31]. Available from: <https://insights.globalspec.com/article/12110/defective-welds-pose-another-setback-for-this-nuclear-power-plant>
- [2] Mineo C, Cerniglia D, Ricotta V, et al. Autonomous 3D geometry reconstruction through robot-manipulated optical sensors. *Int J Adv Manuf Technol.* 2021 Sep;116(5):1895–1911. doi: [10.1007/s00170-021-07432-5](https://doi.org/10.1007/s00170-021-07432-5)
- [3] Foster EA, Bernard R, Bolton G, et al. Inspection of nuclear assets with limited access using feature guided waves. *NDT & E Int.* 2022 Oct;131:102695. doi: [10.1016/j.ndteint.2022.102695](https://doi.org/10.1016/j.ndteint.2022.102695)
- [4] Zhang D, Cao J, Dobie G, et al. A framework of using customized lidar to localize robot for nuclear reactor inspections. *IEEE Sensors J.* 2021 May;22(6):5352–5359. doi: [10.1109/JSEN.2021.3083478](https://doi.org/10.1109/JSEN.2021.3083478)
- [5] Poole A, Sutcliffe M, Pierce G, et al. Autonomous, digital-twin free path planning and deployment for robotic NDT: introducing LPAS: locate, plan, approach, scan using low cost vision sensors. *Appl Sci.* 2022 May;12(10):5288. doi: [10.3390/app12105288](https://doi.org/10.3390/app12105288)
- [6] Poole A, Sutcliffe M, Pierce G, et al. A novel complete-surface-finding algorithm for online surface scanning with limited view sensors. *Sensors.* 2021 Nov;21(22):7692. doi: [10.3390/s21227692](https://doi.org/10.3390/s21227692)
- [7] Ivan V, Garriga-Casanovas A, Merkt W, et al. Autonomous non-destructive remote robotic inspection of offshore assets. Presented at Offshore Technology Conference (OTC 2022); 2–5 May 2022; Houston, Texas, USA. 2020.
- [8] Tabatabaeipour M, Trushkevych O, Dobie G, et al. Application of ultrasonic guided waves to robotic occupancy grid mapping. *Mech Syst Signal Process.* 2022 1;163:108151. doi: [10.1016/j.ymssp.2021.108151](https://doi.org/10.1016/j.ymssp.2021.108151)
- [9] Zhang D, Watson R, MacLeod C, et al. Implementation and evaluation of an autonomous airborne ultrasound inspection system. *Nondestruct Test Eval.* 2022 Jan;37(1):1–21. doi: [10.1080/10589759.2021.1889546](https://doi.org/10.1080/10589759.2021.1889546)
- [10] Ma X, Kuo W-Y, Yang K, et al. A-SEE: active-sensing end-effector enabled probe self-normal-positioning for robotic ultrasound imaging applications. *IEEE Robot Autom Lett.* 2022 Oct;7(4):12475–12482. doi: [10.1109/LRA.2022.3218183](https://doi.org/10.1109/LRA.2022.3218183)
- [11] Jiang Z, Grimm M, Zhou M, et al. Automatic force-based probe positioning for precise robotic ultrasound acquisition. *IEEE Trans Ind Electron.* 2021 Nov;68(11):11200–11211. doi: [10.1109/TIE.2020.3036215](https://doi.org/10.1109/TIE.2020.3036215)
- [12] Delasse C, Lafkiri H, Hajji R, et al. Indoor 3d reconstruction of buildings via azure Kinect RGB-D camera. *Sensors.* 2022 11;22(23):9222. doi: [10.3390/s22239222](https://doi.org/10.3390/s22239222)
- [13] Intel. Intel realsense depth camera d435i. Available from: <https://www.intelrealsense.com/depth-camera-d435i/>
- [14] Mitra NJ, Nguyen A. Estimating surface normals in noisy point cloud data. *Proceedings of the Nineteenth Annual Symposium on Computational Geometry*; San Diego California USA. 2003. p. 322–328.
- [15] Carfagni M, Furferi R, Governi L, et al. Metrological and critical characterization of the intel D415 stereo depth camera. *Sensors.* 2019 Jan;19(3):489. doi: [10.3390/s19030489](https://doi.org/10.3390/s19030489)

- [16] Servi M, Mussi E, Profili A, et al. Metrological characterization and comparison of D415, D455, L515 RealSense devices in the close range. *Sensors*. 2021 Jan;21(22):7770. doi: 10.3390/s21227770
- [17] Chiu C-Y, Thelwell M, Senior T, et al. Comparison of depth cameras for three-dimensional reconstruction in medicine. *Proc Inst Mech Eng H*. 2019 Sep;233(9):938–947. doi: 10.1177/0954411919859922
- [18] Zhang L, Xia H, Qiao Y. Texture synthesis repair of RealSense D435i depth images with object-oriented RGB image segmentation. *Sensors*. 2020 Jan;20(23):6725. doi: 10.3390/s20236725
- [19] Wang T-M, Shih Z-C. Measurement and analysis of depth resolution using active stereo cameras. *IEEE Sensors J*. 2021 Apr;21(7):9218–9230. doi: 10.1109/JSEN.2021.3054820
- [20] Ahn MS, Chae H, Noh D, et al. Analysis and noise modeling of the intel RealSense D435 for Mobile robots. *2019 16th International Conference on Ubiquitous Robots (UR)*; 2019 Jun; Jeju, South Korea. p. 707–711.
- [21] Jonasson ET, Ramos Pinto L, Vale A. Comparison of three key remote sensing technologies for mobile robot localization in nuclear facilities. *Fusion Eng Des*. 2021 Nov;172:112691. doi: 10.1016/j.fusengdes.2021.112691
- [22] Vasilev M, MacLeod CN, Loukas C, et al. Sensor-enabled multi-robot system for automated welding and in-process ultrasonic nde. *Sensors*. 2021 7;21(15):5077. doi: 10.3390/s21155077
- [23] Schnabel R, Wahl R, Klein R. Efficient RANSAC for point-cloud shape detection. *Comput Graphics Forum*. 2007;26(2):214–226. doi: 10.1111/j.1467-8659.2007.01016.x
- [24] Zhang D, Jackson W, Dobie G, et al. Structure-from-motion based image unwrapping and stitching for small bore pipe inspections. *Comput Ind*. 2022 Aug;139:103664. doi: 10.1016/j.compind.2022.103664
- [25] JIREH Industries. Navic. Available from: <https://www.jireh.com/navic/>
- [26] Mecademic. Meca500. Available from: <https://www.mecademic.com/meca500-industrial-robot-arm/>
- [27] ATI Industrial Automation. F/t sensor: mini40. Available from: <https://www.ati-ia.com/>
- [28] Zetec. Ut probes and wedges. Available from: <https://www.zetec.com/products/ultrasound/ut-probes-wedges-and-accessories/>
- [29] Jackson W, Zhang D, McMillan R, et al. Magnetic inspection platform for teleoperated remote inspections of complex geometry. In: 2022 49th annual review of progress in quantitative nondestructive evaluation (QNDE 2022). San Diego, United States: American Society of Mechanical Engineers Digital Collection; 2022 Jul.
- [30] ROS. Robot operating system. Available from: <https://www.ros.org/>
- [31] Zetec. Ut software. 2023. Available from: <https://www.zetec.com/products/ultrasound/software-ut/>
- [32] Rusu RB. Semantic 3D object maps for everyday manipulation in human living environments. *KI - Künstliche Intelligenz*. 2010 Nov;24(4):345–348. doi: 10.1007/s13218-010-0059-6
- [33] Chen Z, Hung JC. Application of quaternion in robot control. *IFAC Proc Volumes*. 1987 Jul;20(5, Part 4):259–263. doi: 10.1016/S1474-6670(17)55326-4
- [34] Zhao T, Zhang D, Watson R, et al. Evaluation of pulse eddy current for autonomous airborne inspections. In: *IEEE Sensors Letters*; 2024. p. 1–4. doi: 10.1109/LSSENS.2024.3424910
- [35] Ramirez-Martinez A, Rodríguez-Olivares NA, Torres-Torres S, et al. Design and validation of an articulated sensor carrier to improve the automatic pipeline inspection. *Sensors*. 2019 Jan;19(6):1394. doi: 10.3390/s19061394
- [36] Li J, Gao W, Wu Y, et al. High-quality indoor scene 3D reconstruction with RGB-D cameras: a brief review. *Comp Visual Media*. 2022 Sep;8(3):369–393. doi: 10.1007/s41095-021-0250-8
- [37] Sun L, Zhao C, Yan Z, et al. A novel weakly-supervised approach for RGB-D-Based nuclear waste object detection. *IEEE Sensors J*. 2019 May;19(9):3487–3500. doi: 10.1109/JSEN.2018.2888815

- [38] Kuan YW, Ee NO, Wei LS. Comparative study of intel R200, Kinect v2, and primesense RGB-D sensors performance outdoors. *IEEE Sensors J.* 2019 Oct;19(19):8741–8750. doi: 10.1109/JSEN.2019.2920976
- [39] Intel. Intel realsense beginner's guide to depth. 2019. Available from: <https://www.intelreal-sense.com/beginners-guide-to-depth/>
- [40] FARO. Faro quantum max scanarms. [2024 Jul 31]. Available from: <https://www.faro.com/en/Products/Hardware/ScanArms>
- [41] CloudCompare. Cloudcompare - 3d point cloud and mesh processing software open source project. [2024 Jul 31]. Available from: <https://www.danielgm.net/cc/>